**12th IFAC Symposium on Computer Applications in Biotechnology**
**The International Federation of Automatic Control**
**16-18, 2013, December. Mumbai, India**

IFAC

# The regulation of glutaminolysis and citric acid cycle activity during mammalian cell cultivation

Markus Rehberg [*] Maria Wetzel [*] Joachim B. Ritter [*]
Udo Reichl [*],[**]

[*] *Max Planck Institute for Dynamics of Complex Technical Systems, Magdeburg, 39106 Germany (Tel: +49-391-6110206; e-mail: rehberg@mpi-magdeburg.mpg.de)*
[**] *Chair of Bioprocess Engineering, Otto von Guericke University Magdeburg, 39106 Germany*

**Abstract:** Glutaminolysis and citric acid cycle generate carbon sources and cellular energy in dependence of the biosynthesis needs. We here introduce a concept which combines a simple and practicable kinetic description of both pathways with a cell growth model to elucidate the influence of extracellular substrates, transport mechanisms and enzyme regulation on the metabolic activity. The derived model focuses on key reactions and replaces complex cellular mechanisms with growth-dependent functions. The uptake of glutamine and glutamate explains, in combination with cell size variations, a peak-like increase in intracellular metabolite pools at day two after inoculation of cells. Additional regulation of citric acid cycle enzymes prevents the degradation of metabolites during stationary growth phase even under substrate limitation. This work reveals possible ways to improve the biotechnological process of cell cultivation and provides a deeper understanding of glutaminolysis and citric acid cycle activity regulation in mammalian cells.

*Keywords:* modeling, glutaminolysis, citric acid cycle, metabolite, cell growth, mammalian cell

## 1. INTRODUCTION

Metabolism is the driving force for cellular life by covering the essential generation of cellular energy and biomass from extracellular substrates. It constitutes the basis for cell growth, and understanding the dynamics in metabolic activity is fundamental for analysis and improvement of biotechnological processes involving mammalian cells, e.g. in vaccine (Genzel et al., 2004) or recombinant protein production (Frame and Hu, 1991b; Fitzpatrick et al., 1993). Substrates for glutaminolysis are the amino acids glutamine and glutamate. The deaminated products fuel the citric acid cycle, which mainly supplies biosynthesis pathways but also generates cellular energy via respiratory activity (Baggetto, 1992; Moreno-Sanchez et al., 2007). Over the last years, quantification of extracellular and intracellular metabolites (Sellick et al., 2011; Dietmair et al., 2012) as well as maximum *in vitro* enzyme activity measurements (Janke et al., 2011) were used to investigate growth and product formation or adaptation of metabolism after changes in media composition. Mathematical models are helpful tools for integration and analysis of such diverse experimental data sets to ultimately conclude on the underlying mechanisms. Apart from metabolic flux analysis (Wahl et al., 2008; Sidorenko et al., 2008) covering steady state conditions, dynamic models (Poertner and Schaefer, 1996; Frame and Hu, 1991a) have been developed to describe extracellular aspects during cell cultivation, e.g. cell growth, substrate consumption and product formation. However, highly structured models, for example *in vitro* bioenergetics of isolated mitochondria (Bazil et al., 2010), are usually too complex for parametrization based upon the limited availability of *in vivo* data. Here, we present a simple and practicable kinetic description of glutaminolysis and citric acid cycle which is linked to a cell growth model to reflect salient features of experimental observations during different growth phases of adherent Madin Darby canine kidney (MDCK) cell cultivation. To elucidate the influence of extracellular substrates, transport mechanisms and enzyme regulation on the metabolic activity, the model integrates data on intracellular metabolite dynamics, maximum *in vitro* enzyme activities and metabolic flux analysis.

## 2. MATERIAL AND METHODS

### 2.1 Cell cultivation and metabolite quantification

Cell cultivation, measurement of cell properties and quantification of extracellular metabolites is in detail described by Rehberg et al. (2013). Data was obtained by performing three independent experiments indicated with symbols $\Delta$, $\square$ and $\circ$. In short, adherent MDCK cells (ECACC, #84121903) were seeded into parallel six-well plates (Greiner Bio-One, #657160) with GMEM medium (Gibco, #22100-093), supplemented with 10% fetal calf serum (Gibco, #10270-106), 2 g/L peptone (International Diagnostics Group, #MC33) and 4 g/L NaHCO$_3$ (Roth, #6885.1). Extracellular metabolites of three wells were analysed using a Bioprofile 100 plus analyser (Nova

Biomedical, relative standard deviation of the methods 1.9-6.4 %), and are presented as mean and standard deviation. Intracellular metabolites were quantified as described by Ritter et al. (2010). In short, the medium of the wells was discarded and cell layers were washed with 0.9 % NaCl solution to remove apoptotic and dead cells in the supernatant. Quenching of metabolic reactions and extraction of metabolites was done by immediate addition of MeOH/CHCl$_3$ solution (1:1). Quantification of the metabolites was performed for three wells by anion exchange chromatography (BioLC system, Dionex) in combination with mass spectrometry (LC-MS, relative standard deviation of the method 0.7 - 9.5 %), as described by (Ritter et al., 2006) and (Ritter et al., 2008), and are presented as mean and standard deviation of the triplicates.

*2.2 Computation*

Model fitting, estimation of the parameters and visualization of the results were programmed in MATLAB® (Version R2010b, The MathWorks, Inc.). Models and data were handled with the Systems Biology Toolbox 2 by (Schmidt and Jirstrand, 2006). For stochastic global optimization of parameters and initial conditions the algorithm fSSm of (Egea et al., 2007) was used. Bootstrapping with 2000 iterations was applied for assessment of parameter confidence intervals (Joshi et al., 2006). All simulations were carried out on a Linux-based system, Intel©Core™ Quad CPU Q6700 @ 2.66GHz and 4 GB memory.

### 3. MODEL

In the following we derive a growth-dependent uptake rate for extracellular glutamate (Glu$^x$) and a release rate for extracellular ammonia (NH$_4^x$) as an extension to the model of Rehberg et al. (2013). In this segregated growth model, cells proceed through the classes $i = 1, ..., 5$ with increasing diameter until they reach the largest class and divide into two cells of the initial class. The transition from the first to the second class is controlled by a cell volume-dependent growth inhibition factor $f$ (-), which limits the volume of all cells with respect to the well surface capacity. The resulting growth phases are identified as follows: exponential growth phase 0-30 h ($1 \geq f \geq 0.95$), intermediate growth phase 30-53 h (onset of growth inhibition to full growth inhibition, $0.95 > f > 0.05$), stationary growth phase 53-200 h ($0.05 \geq f \geq 0$). Furthermore, the model provides the class-specific viable cell numbers X$_i$ (cell), the total viable cell number X$_{tot}$ (cell), the specific growth rate $\mu$ (h$^{-1}$), the cell volume V$^C$ (of all cells, here in L), the medium volume $V^M$ (L), the water evaporation rate constant $F_{evap}$ (L h$^{-1}$) as well as the medium volume-specific uptake rate of extracellular glutamine (Gln$^x$) for growth $r_{X/Gln}$ (mmol L$^{-1}$ h$^{-1}$), and the rate $r_{dGln}$ (mmol L$^{-1}$ h$^{-1}$) describing its spontaneous decomposition. On the extracellular level we now define:

$$\frac{d[Glu^x]}{dt} = -r_{Glu}\frac{V^C}{V^M} + \frac{F_{evap}[Glu^x]}{V^M} \quad (1)$$

$$\frac{d[NH_4^x]}{dt} = 2r_{X/Gln} + r_{dGln} + r_{Glu}\frac{V^C}{V^M} \quad (2)$$

$$- r_{X/NH_4} - r_{m/NH_4} + \frac{F_{evap}[NH_4^x]}{V^M}$$

$$r_{Glu} = K_{GT}[Glu^x](1 - f) \quad (3)$$

$$r_{X/NH_4} = \mu(X_1 f + \sum_{i=2}^{5} X_i)Y_{X/NH_4} \quad (4)$$

$$r_{m/NH_4} = m_{NH_4}V^C\Theta([NH_4^x]) \quad (5)$$

with $K_{GT}$ (h$^{-1}$) as transport rate constant of Glu$^x$, $Y_{X/NH_4}$ (mmol L$^{-1}$ cell$^{-1}$) as cell growth-specific yield coefficient of NH$_4^x$ for growth and $m_{NH_4}$ (mmol L$^{-1}$ L$^{-1}$ cell$^{-1}$) as cell volume-specific uptake rate of NH$_4^x$ for maintenance, with $\Theta([NH_4^x])$ being one for NH$_4^x >$ 0 and zero otherwise. Note, that the rate constants are defined as $K_{Enzyme} = k_{Enzyme}X_{tot}/V^C$ and are, hence, time-dependent cell volume-specific enzyme activities, which also applies in the following for the Michaelis-Menten equations with $K_{Enzyme}^{max} = V_{Enzyme}^{max}X_{tot}/V^C$ (with *Enzyme* as synonym for $GT$, $GDH$, $SDH$, $FMA$, $\alpha DH$, $MDH$). Intracellular metabolite pools of glutamine (Glu), $\alpha$-ketoglutarate ($\alpha$Kg), succinate (Suc), fumarate (Fum) and malate (Mal) are defined as follows:

$$\frac{d[Glu]}{dt} = r_{Glu} + r_{X/Gln}\frac{V^M}{V^C} - K_{GDH}[Glu] \quad (6)$$

$$\frac{d[\alpha Kg]}{dt} = K_{GDH}[Glu] - K_{\alpha DH}[\alpha Kg]b_{syn} \quad (7)$$

$$\frac{d[Suc]}{dt} = K_{\alpha DH}[\alpha Kg]b_{syn} - K_{SDH}([Suc] - \frac{[Fum]}{k_{SDH}^{eq}}) \quad (8)$$

$$\frac{d[Fum]}{dt} = K_{SDH}([Suc] - \frac{[Fum]}{k_{SDH}^{eq}}) \quad (9)$$

$$- K_{FMA}^{max}\frac{[Fum] - \frac{[Mal]}{k_{FMA}^{eq}}}{k_{FMAFum}^m + [Fum] + \frac{[Mal]}{k_{FMA}^{eq}}}$$

$$\frac{d[Mal]}{dt} = K_{FMA}^{max}\frac{[Fum] - \frac{[Mal]}{k_{FMA}^{eq}}}{k_{FMAFum}^m + [Fum] + \frac{[Mal]}{k_{FMA}^{eq}}} \quad (10)$$

$$- K_{MDH}^{max}\frac{[Mal]}{k_{MDHMal}^m + [Mal]}b_{syn}$$

$$b_{syn} = \frac{X_1 f + \sum_{i=2}^{5} X_i}{X_{tot}} \quad (11)$$

With $K_{GDH}$ (h$^{-1}$) as glutamate conversion rate constant by glutamate dehydrogenase and transaminase, $K_{\alpha DH}$(h$^{-1}$) as $\alpha$-ketoglutarate dehydrogenase rate constant, $K_{SDH}$ (h$^{-1}$) as succinate dehydrogenase rate constant and its equilibrium constant $k_{SDH}^{eq}$ (-), $K_{FMA}^{max}$ (mmol L$^{-1}$ cell$^{-1}$) as maximum activity of fumarase with its affinity constant $k_{FMAFum}^m$ (mmol L$^{-1}$) for Fum and its equilibrium constant $k_{FMA}^{eq}$ (-), $K_{MDH}^{max}$ (mmol L$^{-1}$ cell$^{-1}$) as maximum activity of malate dehydrogenase and its affinity constant $k_{MDHMal}^m$ for Mal. $b_{syn}$ is a factor to describe the growth-dependent use of $\alpha$Kg and Mal for biosynthesis.

## 4. RESULTS

### 4.1 Extracellular metabolites

Sources for citric acid cycle intermediates are intracellular glutamine and glutamate while their conversion by glutaminolysis to $\alpha$Kg produces intracellular ammonium which can be used for O-GlcNAcylation (Ryll et al., 1994) or is directly transferred to other amino acids. Glu$^x$ uptake was here dependent on the transporter activity, which was up-regulated when cells were inhibited in growth space. Hence, Glu$^x$ concentrations even increased slightly due to water evaporation until 30 h of cultivation and then sharply decreased until Glu$^x$ was almost depleted (Fig. 1c). In experiment $\circ$ ($t > 54$ h) the Glu$^x$ concentration remained above zero but was below the quantification limit. The model was in good agreement with the experimental data. NH$_4^x$ increased strongly during the growth phase due to Gln$^x$ and Glu$^x$ breakdown and moderately during stationary growth phase due to spontaneous decomposition of Gln$^x$ and water evaporation (Fig. 1d). Experiment $\square$ indicated a stronger increase in NH$_4^x$ during stationary growth phase, which resulted neither from Gln$^x$ nor from Glu$^x$ uptake (note that $r_{X/Gln} = 0$ for $t > 53$ h). Nevertheless, the NH$_4^x$ increase seemed to correlate strongly with Gln$^x$. Furthermore, simulation results indicated a sharp increase in NH$_4^x$ at about 30 h which was not observed experimentally.
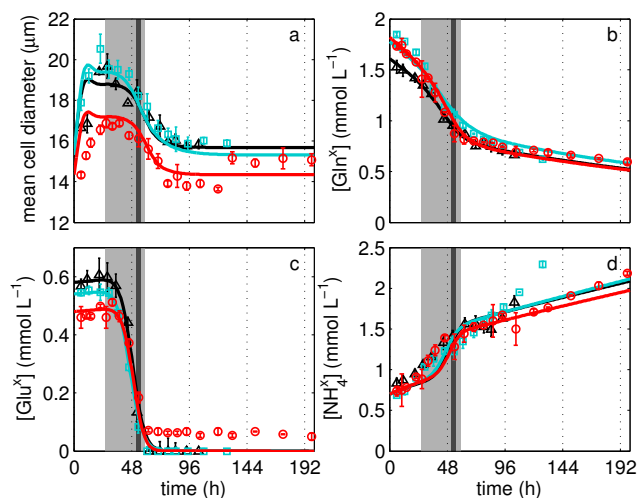


Fig. 1. Growth of adherent MDCK cells in six-well plates in GMEM. Data and model simulation of mean cell diameter (a) and glutamine concentration (b) were taken from Rehberg et al. (2013). Data for glutamate (c) and ammonia (d) of three independent experiments ($\triangle$, $\square$, $\circ$) represent mean and standard deviation of three wells. Lines are respective model simulations. Light grey field between 1-2.5 days of cultivation illustrates the interval of 5 % to 95 % growth inhibition according to Rehberg et al. (2013); black bar indicates the cease of cell volume growth after 2 days

### 4.2 Intermediates of lower citric acid cycle

In the lower citric acid cycle, $\alpha$Kg is mainly converted to Suc and subsequently to Fum and Mal. Mal is then converted to oxaloacetate or transported from the mitochondria into the cytosol. Oxaloacetate is in turn used by aspartate transaminase for the production of $\alpha$Kg from mitochondrial glutamate instead of being transferred into the upper citric acid cycle (Sidorenko et al., 2008). All four citric acid cycle intermediates exhibited a peak-like behavior during cell growth with a maximum around 48 h of cultivation (Fig. 2). In experiment $\triangle$ and $\square$, early levels ($0 < t < 30$ h) of $\alpha$Kg were similar to the levels of stationary growth phase ($t > 53$ h, Fig. 2a-b). But differences were found for experiment $\circ$, where measurements for $\alpha$Kg were systematically higher than in the other two experiments and in the model simulation (Fig. 2c). Also, much lower levels at early times of cultivation than during stationary growth phase were found. In case of Suc, experiment-specific differences were much smaller and early levels were always higher than levels during stationary growth phase (Fig. 2d-f). The model reflected this phenomenon as well as the subsequent peak and the constant level during stationary growth phase. The model simulation of Fum and Mal was in good agreement with experimental observations although it suggested slightly lower concentrations in stationary growth phase (Fig. 2g-l). Analysis of the simulated flux rates revealed a maximum activity of lower citric acid cycle (malate dehydrogenase) of about 29 mmol L$^{-1}$ cell$^{-1}$ (at 48 h), which allows an ATP production from GTP, NADH and FADH$_2$ of 145 mmol L$^{-1}$ cell$^{-1}$ (theoretical maximum). During stationary growth phase, the activity of lower citric acid cycle was zero ($t > 53$ h).

### 4.3 Initial conditions and parameters of glutaminolysis and citric acid cycle

Initial conditions for intracellular metabolites were set to the levels of stationary growth phase ($t = 200$ h) and are thus defined by the internal and external parameters of glutaminolysis and citric acid cycle (Table 1). The

Table 1. Experiment-specific initial conditions for (1), (2) and (6)-(10) as a model extension of Rehberg et al. (2013)

|  | $\triangle$ | $\square$ | $\circ$ | unit |
|---|---|---|---|---|
| $[Glu^x]$ | 0.58 | 0.54 | 0.48 | mmol L$^{-1}$ |
| $[NH_4^x]$ | 0.76 | 0.74 | 0.74 | mmol L$^{-1}$ |
| $[Glu]$ | 0.05 | 0.05 | 0.05 | mmol L$^{-1}$ |
| $[\alpha Kg]$ | 0.19 | 0.19 | 0.19 | mmol L$^{-1}$ |
| $[Suc]$ | 0.11 | 0.11 | 0.11 | mmol L$^{-1}$ |
| $[Fum]$ | 0.04 | 0.04 | 0.04 | mmol L$^{-1}$ |
| $[Mal]$ | 0.32 | 0.32 | 0.32 | mmol L$^{-1}$ |

parameters of this work were estimated by simultaneous fitting of the three experiments according to a model described previously by Rehberg et al. (2013) and are given in Table 2. Optimal parameter values and parameter confidence intervals (Table 2) indicated that the chosen enzyme kinetics as well as the glutamate transport kinetic were well defined by the experimental data. Only, $k_{GDH}$ could not be estimated as measurements for intracellular glutamate were not available. An additional constraint was here that intracellular glutamate levels must be low, which led to potentially higher $k_{GDH}$ values compared to other enzymes. Most notably, $k_{\alpha DG}$, $k_{GT}$ as well as $k_{SDH}$ were

Table 2. Estimated parameter values on the basis of three experiments with confidence intervals between 0.025-quantile ($Q_{0.025}$) and 0.975-quantile ($Q_{0.975}$) derived by a bootstrapping approach (2000 iterations, (Joshi et al., 2006)) for (3)-(10) as a model extension of Rehberg et al. (2013)

| param. | value | $Q_{0.025} - Q_{0.975}$ | unit | param. | value | $Q_{0.025} - Q_{0.975}$ | unit |
|---|---|---|---|---|---|---|---|
| $k_{\alpha DH}$ | $2.10 \times 10^{-10}$ | $(1.89 - 2.36) \times 10^{-10}$ | L cell$^{-1}$ h$^{-1}$ | $k^m_{FMAFum}$ | $2.06$ | $1.01 - 3.15$ | mmol L$^{-1}$ |
| $k_{GDH}$ | $2.09 \times 10^{-10}$ | $(0.32 - 5.55) \times 10^{-8}$ | L cell$^{-1}$ h$^{-1}$ | $k^m_{MDHMal}$ | $4.52 \times 10^2$ | $(4.13 - 4.72) \times 10^2$ | mmol L$^{-1}$ |
| $k_{GT}$ | $3.13 \times 10^{-10}$ | $(2.70 - 3.56) \times 10^{-10}$ | L cell$^{-1}$ h$^{-1}$ | $m_{NH_4}$ | $2.44 \times 10^{-10}$ | $(0.00 - 2.06) \times 10^{-8}$ | mmol L$^{-1}$ L$^{-1}$ h$^{-1}$ |
| $k_{SDH}$ | $5.71 \times 10^{-10}$ | $(0.41 - 1.29) \times 10^{-9}$ | L cell$^{-1}$ h$^{-1}$ | $V^{max\ a}_{FMA}$ | $5.54 \times 10^{-9}$ | $-$ | mmol cell$^{-1}$ h$^{-1}$ |
| $k^{eq}_{FMA}$ | $7.44$ | $6.67 - 8.04$ | $-$ | $V^{max\ a}_{MDH}$ | $5.63 \times 10^{-8}$ | $-$ | mmol cell$^{-1}$ h$^{-1}$ |
| $k^{eq}_{SDH}$ | $0.40$ | $0.36 - 0.45$ | $-$ | $Y_{X/NH_4}$ | $5.62 \times 10^{-7}$ | $(5.50 - 5.74) \times 10^{-7}$ | mmol L$^{-1}$ cell$^{-1}$ |

[a] measured *in vitro* by Janke et al. (2011)
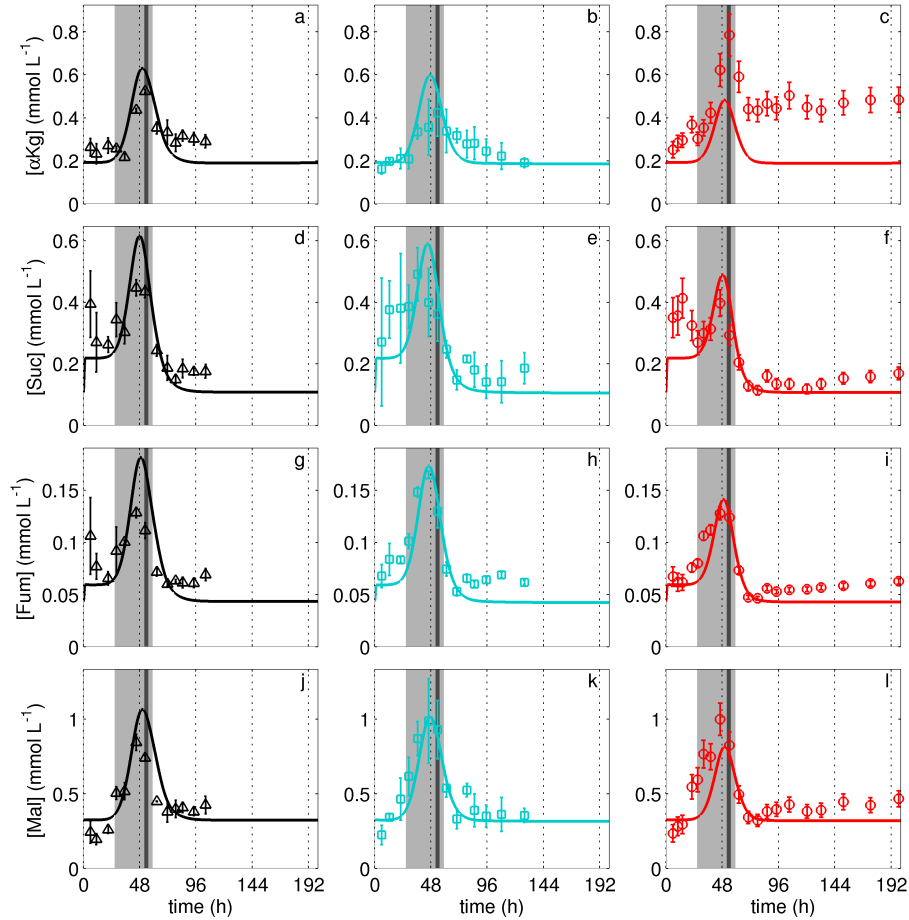


Fig. 2. Intracellular metabolite pools of lower citric acid cycle during growth of adherent MDCK cells in six-well plates in GMEM. Time series of $\alpha$-ketoglutarate (a, b, c), succinate (d, e, f), fumarate (g, h, i) and malate (j, k, l) are shown for the three experiments ($\Delta$, $\square$, $\circ$) as mean and standard deviation of three wells. Model simulations are based on Rehberg et al. (2013) with an extension by (1)-(11) and parameters of Table 1 and Table 2. Light grey field between 1-2.5 days of cultivation illustrates the interval of 5 % to 95 % growth inhibition according to Rehberg et al. (2013); black bar indicates the cease of cell volume growth after 2 days.

in the same activity range. Comparing the Fum and Mal concentrations of this work with $k^m_{FMAFum}$ and $k^m_{MDHMal}$, respectively, revealed that Michaelis-Menten kinetics were exclusively in the linear range.

## 5. DISCUSSION

In the following we evaluate only key aspects of the developed model and focus afterward on the biological and biotechnological implications of the results.

### 5.1 Model

In this work we coupled a kinetic description of the metabolic pathways glutaminolysis and lower citric acid cycle to a segregated model for cell growth to describe the experimentally measured metabolite pool dynamics. The coupling allowed dealing with mechanistic parts of the glutamate transporter and the metabolic ammonium consumption not explicitly considered in the model by using empiric growth-dependent functions. Additionally,

the model coupling allowed us to consider the influence of cell size (cell-specific volume $V^C/X_{tot}$) variations on intracellular metabolite pools: - firstly, the dilution of intracellular metabolites, which was neglected as it was a few magnitudes smaller than the actual flux rates - secondly, the implementation of cell number-based enzyme activities and maximum *in vitro* enzyme activities. In particular, the relation of both to the cell-specific volume introduced an additional dynamic, which also shaped in our model the behavior of intracellular metabolite pools. In conclusion, the cell number-based activity is varying differently between the growth phase and the stationary growth phase than the cell-specific volume (Janke et al., 2011). Enzyme kinetics of glutaminolysis and lower citric acid cycle were described by conventional mass-action and Michaelis-Menten kinetics to derive a simple but, in a biological sense, still reasonable set of differential equations that focus on key regulatory mechanisms. Cofactors such as GTP, FAD as well as amino acid breakdown and amino acid synthesis were not considered in this study (except for $Gln^x$, $Glu^x$) but could potentially also contribute to the observed dynamics of metabolite pools. Instead, we implemented $b_{syn}$ as a factor to describe the growth-dependent use of citric acid cycle intermediates for biomass synthesis. Note that $b_{syn}$ may represent one of these cofactors (see 5.3 for further discussion). So far, the upper part of the citric acid cycle is neglected in this work as it is largely disconnected in MDCK cells from the lower part (Sidorenko et al., 2008). This "truncated citric acid cycle" is a widely known phenomenon, which is comprehensively reviewed by Moreno-Sanchez et al. (2007) and is also described for other continuous cell lines (Niklas et al., 2011).

### 5.2 Glutaminolysis activity based on metabolite fluxes

In addition to the growth-dependent uptake of $Gln^x$, the uptake of $Glu^x$ was described by a glutamate transport kinetic modulated by the growth inhibition factor $f$. Therefore, uptake of $Glu^x$ started with onset of the intermediate growth phase ($t > 30$ h) which corresponds to experimental observations of Genzel et al. (2005) for MDCK cells grown in roller bottles. The release of $NH_4^x$ was described by the maximum stoichiometric production from $Gln^x$ and $Glu^x$ uptake minus the consumption for cell growth and cell maintenance. The model suggested a negligible $m_{NH_4}$, which implies that $NH_4^x$ is only consumed for biomass growth and is not required for the maintenance of biomass. Also, glutamine is only used for biomass growth (Rehberg et al., 2013). In the present form of the model, the stepwise change in $NH_4^x$ release at about 30 h was not in agreement with experimental observations. If $NH_4^x$ release resulted only from $Gln^x$ uptake, the fit was markedly improved (data not shown). This indicates that major amounts of the $Glu^x$ were processed via the transamination route without production of free $NH_4^x$. A high transaminase activity (in the range of the fumarase activity) is indeed present in MDCK cells (Janke et al., 2011). In contrast to $Glu^x$, $Gln^x$ seemed to be transported into the mitochondria and then converted to $\alpha Kg$ under the production of mitochondrial ammonium. Secretion of ammonium into the medium can have a negative impact on cell growth and product formation at least at higher concentrations (Butler et al., 1983). As both $Gln^x$ and $Glu^x$ fuel the citric acid cycle, cultivation processes with

high $NH_4^x$ accumulation may benefit from corresponding media adaptation (Butler et al., 1983; Genzel et al., 2005) or a modulation of the cellular transporters in favor of $Glu^x$ uptake.

### 5.3 Regulation of lower citric acid cycle

As cells from stationary growth phase were used for inoculation of a new well, we assumed that initial metabolite levels ($t = 0$) correspond to levels of stationary growth phase. For Fum and Suc, the model suggested a fast increase in the concentration due to $Gln^x$ uptake and breakdown. In consequence, early intracellular levels were higher than levels of stationary growth phase (Fig. 2). This phenomenon was not observed for $\alpha Kg$ and Mal because breakdown is controlled by $b_{syn}$ and depends only partially on the metabolite levels of cells in the stationary growth phase. After the first 30 h, however, a peak-like behavior was found for all measured intracellular metabolites, which was to a large extend caused by the $Glu^x$ uptake during the intermediate growth phase. It seemed that growth-dependent uptake rates modulated the intracellular metabolite pools during cultivation as long as extracellular substrates were available in sufficient amounts. Similar observations are made for the glycolytic pathway of rat thymus lymphocytes where the glucose transporter is activated experimentally (Yasmeen et al., 1977), and is also expected for metabolism of tumor cells (Macheda et al., 2005). The resulting highly dynamic metabolic behavior during the typical course of cultivations complicates the application of metabolic flux analysis (which assumes typically stationary conditions during exponential growth at $\mu_{max}$) considerably and underlines the need for simple kinetic models that capture such growth-dependent changes. During the stationary growth phase neither $Gln^x$ nor $Glu^x$ were consumed but the metabolite pools of the citric acid cycle remained constant. Therefore, either breakdown of other amino acid fueled the citric acid cycle or enzyme activities were down-regulated. No efforts were taken, so far, to further increase the complexity of the model as experimental data were fitted with sufficient accuracy. Instead, it was simply assumed that the metabolism may regulate $\alpha$-ketoglutarate dehydrogenase and malate dehydrogenase in dependence of the biosynthesis needs ($b_{syn}$) to prevent an overproduction of biomass precursors. Interestingly, both enzymes have the cofactor $NAD^+$ in common, which is indeed a metabolic regulator (Bazil et al., 2010). The fact that the model allowed to fit the constant metabolite levels during stationary growth phase sufficiently, suggests that enzyme regulation plays an additional role in down-regulation of the citric acid cycle activity. This might help to stabilize intracellular concentrations of metabolic intermediates by enzyme regulation when specific metabolites (such as $Glu^x$) are depleted to critical levels. Furthermore, we anticipate that the regulation of enzymes to reduce citric acid cycle activity is an intrinsic mechanism under a stationary growth regime where the cell switches to a reduced $Gln^x$ uptake. From the flux rates through $\alpha$-ketoglutarate dehydrogenase and succinate dehydrogenase, we calculated a theoretical maximum ATP production that can reach 30 % of glycolytic ATP production during the exponential growth phase and up to 70 % during the intermediate growth phase (unpublished data). A higher ATP production by glycolysis compared to the

citric acid cycle is also calculated by Wahl et al. (2008) using metabolic flux analysis. However, increasing the Glu$^x$ uptake may enhance ATP production but more importantly lipid-synthesis from Mal-derived NADPH, which might effect $\mu_{max}$ in a positive way. Furthermore, a shift towards higher lipid synthesis might be important for the production of enveloped viruses (Munger et al., 2008). At least the maximum *in vitro* enzyme activities of fumarase and malate dehydrogenase indicate a significant additional capacity for metabolite conversion.

## 6. CONCLUSION

The derived model consists of simple but, in a biological sense, still reasonable kinetics for key reactions of glutaminolysis and citric acid cycle which are linked to a comprehensive model description of cell growth phases. By replacing complex biological mechanisms with growth-dependent functions, the model explained intracellular metabolite pool dynamics during growth of adherent cells and revealed the interplay of uptake rates and intrinsic enzyme regulation. Finally, the model suggested that an increase in glutamate uptake during growth by molecular biological tools could contribute to the improvement of cell culture processes by reducing ammonium accumulation and enhancing lipid synthesis. In addition, and more importantly, it allowed a thorough and cause-driven analysis of glutaminolysis and citric acid cycle activity during mammalian cell growth.

REFERENCES

Baggetto, L.G. (1992). Deviant energetic metabolism of glycolytic cancer cells. *Biochimie*, 74(11), 959–974.

Bazil, J.N., Buzzard, G.T., and Rundell, A.E. (2010). Modeling mitochondrial bioenergetics with integrated volume dynamics. *Plos Computational Biology*, 6(1), e1000632.

Butler, M., Imamura, T., Thomas, J., and Thilly, W.G. (1983). High yields from microcarrier cultures by medium perfusion. *J Cell Sci*, 61, 351–363.

Dietmair, S., Hodson, M.P., Quek, L.E., Timmins, N.E., Chrysanthopoulos, P., John, S.S., Gray, P., and Nielsen, L.K. (2012). Metabolite profiling of cho cells with different growth characteristics. *Biotechnol Bioeng*. doi:10.1002/bit.24496. URL http://dx.doi.org/10.1002/bit.24496.

Egea, J.A., Rodriguez-Fernandez, M., Banga, J.R., and Marti, R. (2007). Scatter search for chemical and bio-process optimization. *Journal of Global Optimization*, 37 (3), 481–503.

Fitzpatrick, L., Jenkins, H.A., and Butler, M. (1993). Glucose and glutamine metabolism of a murine b-lymphocyte hybridoma grown in batch culture. *Appl Biochem Biotechnol*, 43(2), 93–116.

Frame, K.K. and Hu, W.S. (1991a). Kinetic study of hybridoma cell growth in continuous culture. i. a model for non-producing cells. *Biotechnol Bioeng*, 37(1), 55–64. doi:10.1002/bit.260370109. URL http://dx.doi.org/10.1002/bit.260370109.

Frame, K.K. and Hu, W.S. (1991b). Kinetic study of hybridoma cell growth in continuous culture: Ii. behavior of producers and comparison to nonproducers. *Biotechnol Bioeng*, 38(9), 1020–1028. doi:10.1002/bit.260380910. URL http://dx.doi.org/10.1002/bit.260380910.

Genzel, Y., Behrendt, I., Knig, S., Sann, H., and Reichl, U. (2004). Metabolism of mdck cells during cell growth and influenza virus production in large-scale microcarrier culture. *Vaccine*, 22(17-18), 2202–2208. doi:10.1016/j.vaccine.2003.11.041. URL http://dx.doi.org/10.1016/j.vaccine.2003.11.041.

Genzel, Y., Ritter, J.B., Knig, S., Alt, R., and Reichl, U. (2005). Substitution of glutamine by pyruvate to reduce ammonia formation and growth inhibition of mammalian cells. *Biotechnol Prog*, 21(1), 58–69. doi:10.1021/bp049827d. URL http://dx.doi.org/10.1021/bp049827d.

Janke, R., Genzel, Y., Hndel, N., Wahl, A., and Reichl, U. (2011). Metabolic adaptation of mdck cells to different growth conditions: effects on catalytic activities of central metabolic enzymes. *Biotechnol Bioeng*, 108(11), 2691–2704. doi:10.1002/bit.23215. URL http://dx.doi.org/10.1002/bit.23215.

Joshi, M., Seidel-Morgenstern, A., and Kremling, A. (2006). Exploiting the bootstrap method for quantifying parameter confidence intervals in dynamical systems. *Metab Eng*, 8(5), 447–455. doi:10.1016/j.ymben.2006.04.003. URL http://dx.doi.org/10.1016/j.ymben.2006.04.003.

Macheda, M.L., Rogers, S., and Best, J.D. (2005). Molecular and cellular regulation of glucose transporter (glut) proteins in cancer. *J Cell Physiol*, 202(3), 654–662. doi:10.1002/jcp.20166. URL http://dx.doi.org/10.1002/jcp.20166.

Moreno-Sanchez, R., Rodriguez-Enriquez, S., Marin-Hernandez, A., and Saavedra, E. (2007). Energy metabolism in tumor cells. *FEBS J*, 274(6), 1393–1418. doi:10.1111/j.1742-4658.2007.05686.x. URL http://dx.doi.org/10.1111/j.1742-4658.2007.05686.x.

Munger, J., Bennett, B.D., Parikh, A., Feng, X.J., McArdle, J., Rabitz, H.A., Shenk, T., and Rabinowitz, J.D. (2008). Systems-level metabolic flux profiling identifies fatty acid synthesis as a target for antiviral therapy. *Nat Biotechnol*, 26(10), 1179–1186. doi:10.1038/nbt.1500. URL http://dx.doi.org/10.1038/nbt.1500.

Niklas, J., Schrder, E., Sandig, V., Noll, T., and Heinzle, E. (2011). Quantitative characterization of metabolism and metabolic shifts during growth of the new human cell line age1.hn using time resolved metabolic flux analysis. *Bioprocess Biosyst Eng*, 34(5), 533–545. doi:10.1007/s00449-010-0502-y. URL http://dx.doi.org/10.1007/s00449-010-0502-y.

Poertner, R. and Schaefer, T. (1996). Modelling hybridoma cell growth and metabolism–a comparison of selected models and data. *J Biotechnol*, 49(1-3), 119–135.

Rehberg, M., Ritter, J.B., Genzel, Y., Flockerzi, D., and Reichl, U. (2013). The relation between growth phases, cell volume changes and metabolism of adherent cells during cultivation. *J Biotechnol*. doi:10.1016/j.jbiotec.2013.01.018. URL http://dx.doi.org/10.1016/j.jbiotec.2013.01.018.

Ritter, J.B., Genzel, Y., and Reichl, U. (2008). Simultaneous extraction of several metabolites of energy metabolism and related substances in mammalian cells: optimization using experimental design. *Anal Biochem*, 373(2), 349–69. doi:10.1016/j.ab.2007.10.037. URL http://dx.doi.org/10.1016/j.ab.2007.10.037.

Ritter, J.B., Genzel, Y., and Reichl, U. (2006). High-performance anion-exchange chromatography using on-line electrolytic eluent generation for the determination of more than 25 intermediates from energy metabolism of mammalian cells in culture. *J Chromatogr B Analyt Technol Biomed Life Sci*, 843(2), 216–26. doi:10.1016/j.jchromb.2006.06.004. URL http://dx.doi.org/10.1016/j.jchromb.2006.06.004.

Ritter, J.B., Wahl, A.S., Freund, S., Genzel, Y., and Reichl, U. (2010). Metabolic effects of influenza virus infection in cultured animal cells: Intra- and extracellular metabolite profiling. *BMC Syst Biol*, 4, 61. doi:10.1186/1752-0509-4-61. URL http://dx.doi.org/10.1186/1752-0509-4-61.

Ryll, T., Valley, U., and Wagner, R. (1994). Biochemistry of growth inhibition by ammonium ions in mammalian cells. *Biotechnol Bioeng*, 44(2), 184–193. doi:10.1002/bit.260440207. URL http://dx.doi.org/10.1002/bit.260440207.

Schmidt, H. and Jirstrand, M. (2006). Systems biology toolbox for matlab: a computational platform for research in systems biology. *Bioinformatics*, 22(4), 514–515. doi:10.1093/bioinformatics/bti799. URL http://dx.doi.org/10.1093/bioinformatics/bti799.

Sellick, C.A., Croxford, A.S., Maqsood, A.R., Stephens, G., Westerhoff, H.V., Goodacre, R., and Dickson, A.J. (2011). Metabolite profiling of recombinant cho cells: designing tailored feeding regimes that enhance recombinant antibody production. *Biotechnol Bioeng*, 108(12), 3025–3031. doi:10.1002/bit.23269. URL http://dx.doi.org/10.1002/bit.23269.

Sidorenko, Y., Wahl, A., Dauner, M., Genzel, Y., and Reichl, U. (2008). Comparison of metabolic flux distributions for MDCK cell growth in glutamine- and pyruvate-containing media. *Biotechnol Prog*, 24(2), 311–20. doi:10.1021/bp0702673. URL http://dx.doi.org/10.1021/bp0702673.

Wahl, A., Sidorenko, Y., Dauner, M., Genzel, Y., and Reichl, U. (2008). Metabolic flux model for an anchorage-dependent MDCK cell line: characteristic growth phases and minimum substrate consumption flux distribution. *Biotechnol Bioeng*, 101(1), 135–52. doi:10.1002/bit.21873. URL http://dx.doi.org/10.1002/bit.21873.

Yasmeen, D., Laird, A.J., Hume, D.A., and Weidemann, M.J. (1977). Activation of 3-o-methyl-glucose transport in rat thymus lymphocytes by concanavalin a. temperature and calcium ion dependence and sensitivity to puromycin but to cycloheximide. *Biochim Biophys Acta*, 500(1), 89–102.